POLITECNICO DI TORINO
Repository ISTITUZIONALE

Scale-dependent maximum reinforcement percentage in reinforced concrete beams

Original
Scale-dependent maximum reinforcement percentage in reinforced concrete beams / Carpinteri, A.; Accornero, F.; Cafarelli, R.. - In: STRUCTURAL CONCRETE. - ISSN 1464-4177. - STAMPA. - (2021), pp. 1-12. [10.1002/suco.202000573]

Availability:
This version is available at: 11583/2903436 since: 2021-05-31T12:33:31Z

Publisher:
John Wiley and Sons

Published
DOI:10.1002/suco.202000573

Terms of use:

This article is made available under terms and conditions as specified in the corresponding bibliographic description in the repository

Publisher copyright

(Article begins on next page)

12 October 2024

Check for updates

Received: 9 September 2020 | Revised: 22 March 2021 | Accepted: 23 April 2021

DOI: 10.1002/suco.202000573

TECHNICAL PAPER

fib CEB-FIP WILEY

Scale-dependent maximum reinforcement percentage in reinforced concrete beams

Alberto Carpinteri | **Federico Accornero** | **Renato Cafarelli**

Politecnico di Torino, Department of Structural, Geotechnical, and Building Engineering, 24, C.so Duca degli Abruzzi, Turin, Italy

Correspondence
Federico Accornero, Politecnico di Torino, Department of Structural, Geotechnical, and Building Engineering, 24 C.so Duca degli Abruzzi, 10129 Turin, Italy.
Email: federico.accornero@polito.it

Abstract

The Cohesive/Overlapping Crack Model is able to describe the transition between cracking and crushing failures occurring in reinforced concrete beams by increasing beam depth and/or steel percentage. Within this Nonlinear Fracture Mechanics model, the tensile and compressive ultimate behaviors of the concrete matrix are modeled through two different process zones that advance independently one of another. Moreover, this model is able to investigate local mechanical instabilities occurring in the structural behavior of reinforced concrete structures: tensile snap-back and snap-through, which are due to concrete cracking or steel fracture, and the compressive snap-back occurring at the end of the plastic plateau, which is generated by the unstable growth of the crushing zone. In this context, the application of the Cohesive/Overlapping Crack Model highlights that the ductility, which is represented by the plastic rotation capacity of a reinforced concrete element subjected to bending, decreases as reinforcement percentage and/or beam depth increase. Thus, a scale-dependent maximum reinforcement percentage beyond which concrete crushing occurs prior to steel yielding is demonstrated to exist. In particular, the maximum steel percentage results to be inversely proportional to $h^{0.25}$, h being the beam depth. In this way, a rational and quantitative definition of over-reinforcement is provided as a steel percentage depending on the beam depth.

KEYWORDS

concrete crushing, ductile-to-brittle transition, maximum reinforcement, nonlinear fracture mechanics, reinforced concrete, scale effects

1 | INTRODUCTION

The flexural behavior of a reinforced concrete (RC) beam is heavily influenced by nonlinear phenomena that are usually observed during laboratory tests (Figure 1), although not properly taken into account during the RC design process. More precisely, after the first cracking load, $P_{cr,}$ is reached, a loss of stability is revealed due to a

Discussion on this paper must be submitted within two months of the print publication. The discussion will then be published in print, along with the authors' closure, if any, approximately nine months after the print publication.

This is an open access article under the terms of the Creative Commons Attribution License, which permits use, distribution and reproduction in any medium, provided the original work is properly cited.
© 2021 The Authors. *Structural Concrete* published by John Wiley & Sons Ltd on behalf of International Federation for Structural Concrete.

local reduction in the resistance capacity of the beam. This unstable branch represents a snap-back instability,[1–6] and its severity has been proved to be a function of the mechanical and geometrical characteristics of the structure, as demonstrated by Carpinteri[2,3,7] by means of the brittleness number s_E. After concrete cracking, an ascending branch generated by the steel reinforcement activation is registered. Then, at the end of the plastic plateau (Figure 1), a second snap-back can be revealed, due to the unstable propagation of the crushing zone in the concrete matrix.

In the study of RC fracturing process, the Bridged Crack Model[5,7–10] proved to be able to capture the loading drops due to cracking, particularly in the case of lightly reinforced or high-performance concrete elements. More recently, an extended version of the Bridged Crack Model[11,12] was applied to investigate the scale-transitional role of the shearing failure in RC beams.

Extensive experimental tests have demonstrated that the parameters influencing the ductility of RC elements may be summarized into three main groups: construction material; structural geometry; static system.[13] In this framework, a decrease in the plastic rotation capacity together with an increase in specimen depth and/or reinforcement percentage has been recognized.[14–16] Nevertheless, a large scatter in experimental data has been observed and a comprehensive theory that is able to predict thoroughly the plastic rotation capacity developed by RC members has not been still provided.[17,18]

On the other hand, the Cohesive/Overlapping Crack Model is a Nonlinear Fracture Mechanics application that is able to describe the transition between cracking and crushing failure in RC beams, highlighting a strong correlation between structural behavior, scale, and reinforcement percentage.[6,19–21] In the present paper, the Cohesive/Overlapping Crack Model together with a dimensional analysis approach are adopted in order to define an effective scale-dependent maximum reinforcement percentage for RC beams in flexure.

2 | THE COHESIVE/ OVERLAPPING CRACK MODEL

The Cohesive Crack Model has been widely applied to simulate the damage process zone ahead of the crack tip in concrete structures.[1–3,22–24] According to this model, the material behaves elastically during the first loading stage (Figure 2(a)), whereas in the zone where the principal stress reaches the tensile strength, σ_t, the process zone starts developing.[25] Within this zone, a cohesive law (Figure 2(b)) in the form σ-w^t, σ being the applied stress and w^t the crack opening, is adopted. Stresses apply until

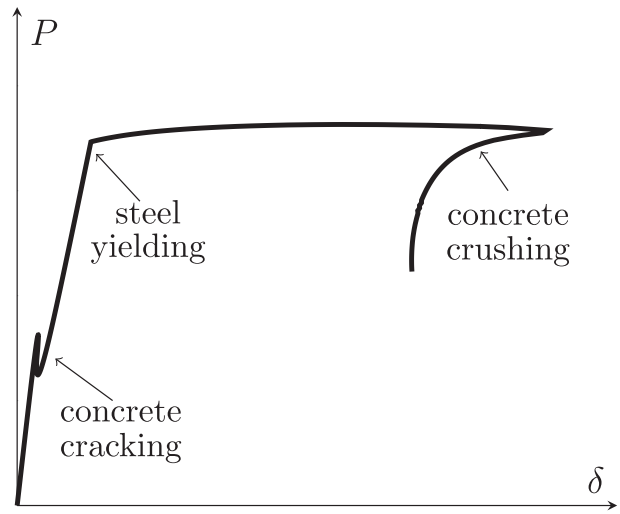

FIGURE 1 Structural behavior of a reinforced concrete beam subjected to bending

the critical value of crack opening, $w^t_{cr,}$ is reached: beyond this limit, the crack faces assume a stress-free condition.

In the present paper, a cohesive constitutive law in the form:

$$\sigma = \sigma_t \left(1 - \frac{w^t}{w^t_{cr}}\right) \tag{1}$$

is assumed. The area subtended by the σ-w^t curve represents the fracture energy, G_F (Figure 2(b)).

Different experimental investigations carried out by Kotsovos,[26] van Mier,[27] Vonk et al.[28] pointed out that concrete exhibits strain localization in compression in a similar way as in tension. In 1997, the RILEM Committee 148-SSC[29] developed an effective standard test for the assessment of the strain softening behavior of concrete under uniaxial compression. The test program, organized by this Committee, involved two different loading conditions and several specimen geometries with different concrete grades were investigated. It was demonstrated that the maximum compressive load in the σ-ε diagram can represent a bifurcation point for the equilibrium path depending on the specimen size and slenderness: an increment in the global ductility was observed with a decrement in the specimen slenderness. Thus, it was concluded that a single σ-ε relationship may not be assumed as an effective constitutive law for concrete in compression in the post-peak regime. On the other hand, it emerged that, if an overlapping relative displacement, w^c, is considered rather than the compressive strain, all the curves converge within a narrow band.[30] The main conclusion of the RILEM round-robin was that two different constitutive laws must be adopted for concrete in compression. In the uncracked stage, the material behavior is described appropriately by a

σ-ε constitutive law (Figure 3(a)) up to the compressive strength σ_c. Beyond that limit, a σ-w^c law must be adopted. The area subtended by the σ-w^c curve (Figure 3(b)) may be interpreted, in close analogy to Figure 2(b), as the crushing energy, G_c, i.e., a compressive fracture energy.[31]

In such a context, Akiyama et al.[32] and Suzuki et al.[33] conducted several tests on plain and laterally-confined concrete specimens, proposing a formula for the determination of G_c. In the case of plain concrete, they suggested the following expression:

$$G_c = 80 - 50k_b \tag{2}$$

with $k_b = 40/\sigma_c < 1$.

Based on these experimental evidence, Carpinteri et al.[34] introduced the Overlapping Crack Model to simulate the post-peak compressive behavior of RC beams in bending. Such model is analogous to the Cohesive Crack Model in tension, since in the elastic stage the concrete behavior is described by a σ-ε constitutive law (Figure 3 (a)), whereas, beyond the peak load, a stress versus fictitious overlapping relationship, σ-w^c, is adopted. This post-peak softening law can thoroughly describe concrete crushing and material expulsion by a fictitious interpenetration.[31]

In the present paper, a linear overlapping law in the form:

$$\sigma = \sigma_c\left(1 - \frac{w^c}{w^c_{cr}}\right) \tag{3}$$

is adopted.

Within the Cohesive/Overlapping Crack Model[21,35–37] the cracking process zone (Figure 4(a)) tends to propagate from the intrados to the extrados of the beam, whereas, vice-versa, the crushing process zone tends to propagate from the extrados to the intrados of the beam (Figure 4(b)). Thus, cracking and crushing failures are modeled as two separate mechanisms, independently evolving and mutually competing.

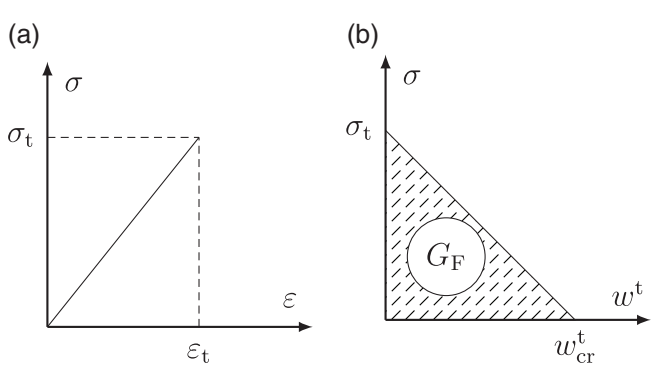

FIGURE 2 Cohesive Crack Model for concrete in tension: (a) linear elastic stress–strain law; (b) post-peak σ-w^t relationship

By means of this Nonlinear Fracture Mechanics Model, the RC beam cross-section is discretized into n different nodal points, being $n = 161$ in order to avoid numerical instabilities, as suggested by Carpinteri et al.[38] For these nodes, the following equation applies:

$$\{w\} = [K_F]\{F\} + \{K_M\}M \tag{4}$$

$\{w\}$ being the vector containing the crack opening/overlapping displacements, $[K_F]$ the matrix containing the coefficients of influence for the nodal displacements generated by the unit nodal forces, $\{K_M\}$ the vector containing the nodal displacements generated by a unit bending moment, and M the value of the applied bending moment. The number of the unknowns in Equation 4 is equal to $(2n + 1)$: n crack opening/overlapping displacements, n nodal forces, and the applied bending moment, M (Figure 5). In addition to Equation 4, the following conditions should be taken into account to describe the RC beam cross-section behavior:

$$F_i = 0 \quad \text{for } i = 1, \ldots, \ (j-1), i \neq r \tag{5a}$$

$$F_i = F_t\left(1 - \frac{w_i}{w^t_{cr}}\right) \quad \text{for } i = j, \ldots, (m-1) \tag{5b}$$

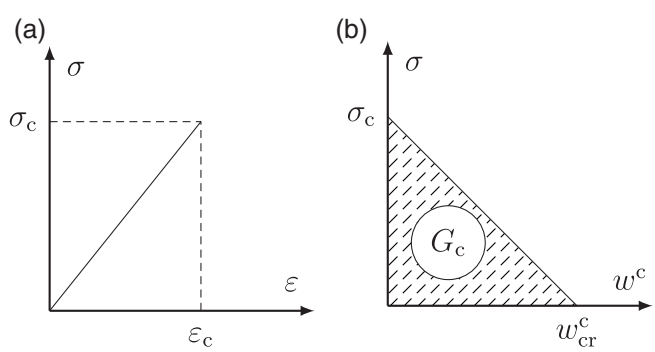

FIGURE 3 Overlapping Crack Model for concrete in compression: (a) linear elastic stress–strain law; (b) post-peak stress versus fictitious interpenetration relationship

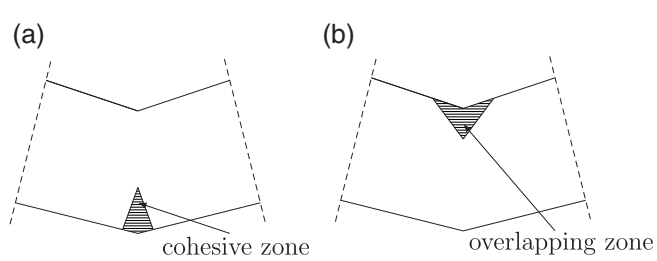

FIGURE 4 Cohesive/Overlapping crack model: (a) Cohesive Crack Model in tension; (b) Overlapping Crack Model in compression

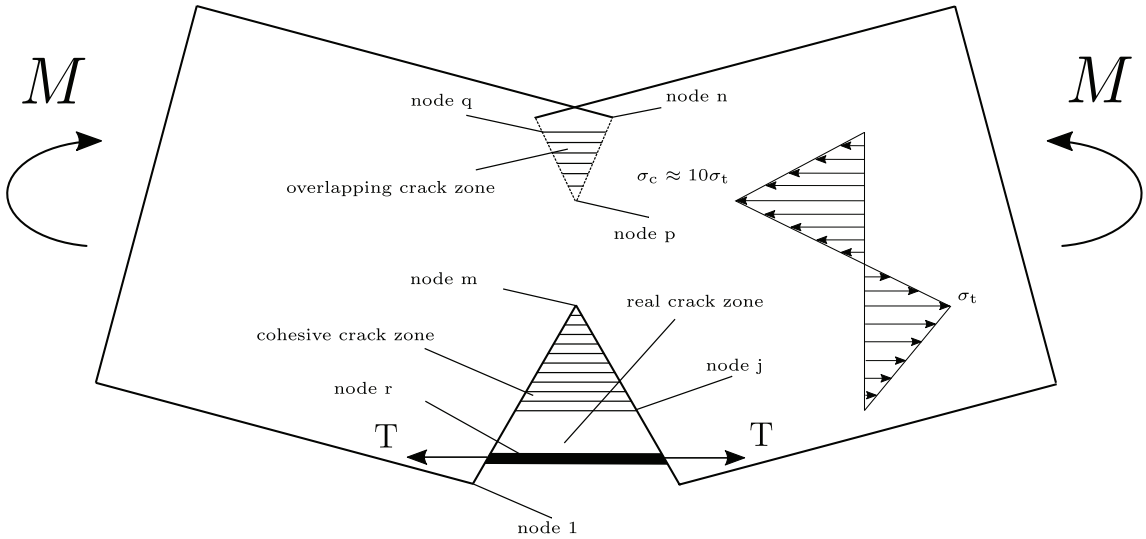

FIGURE 5 Cohesive/overlapping crack model

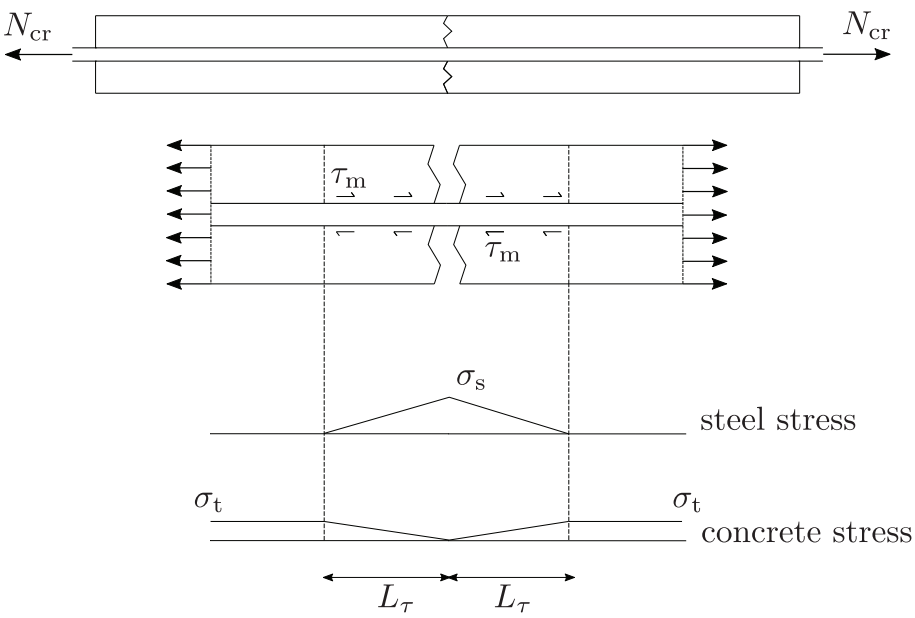

FIGURE 6 Steel-concrete interaction

$$w_i = 0 \quad \text{for} \quad i = m, \ldots, p \tag{5c}$$

$$F_i = F_c\left(1 - \frac{w_i}{w_{cr}^c}\right) \quad \text{for} \quad i = (p+1), \ldots, q \tag{5d}$$

$$F_i = 0 \quad \text{for} \quad i = (q+1), \ldots, n \tag{5e}$$

$$F_i = f(w_i) \quad \text{for} \quad i = r \tag{5f}$$

j being the real crack tip, m the fictitious crack tip, p the fictitious overlapping crack tip, q the real overlapping crack tip, and r the node where the reinforcement layer is located.

Equation 5f correlates the crack opening at the level of reinforcement with the force exerted by the steel bar. This equation can be calibrated according to a bond-slip law proposed in Ruiz and Planas[24], Ruiz[23], Model Code 2010[39]. In Figure 6 it is possible to recognize the length $2L_\tau$, along which concrete and steel mutually transfer the shearing stress $\tau(x)$. The value of L_τ may be calculated by means of the equilibrium condition of the steel bar. Thus, in the case of over-reinforced concrete beams and neglecting the tension stiffening effect, we have:[40,41]

$$\sigma_s A_s = \int_0^{L_\tau} \pi \phi \tau(x) \mathrm{d}x \tag{6}$$

The variation of τ along L_τ depends on concrete strength, steel surface condition, and slippage between these two materials. Thus, in order to simplify Equation 6, it is possible to consider the mean value of the shearing stresses, τ_m, leading to:

$$L_\tau = \frac{\sigma_S A_S}{\pi \phi \tau_m} \leq \ell/2 \tag{7}$$

where ℓ is the beam span.

Then, the value of the crack opening, w^t, may be obtained as:

$$w^t = 2\int_0^{L_\tau} [\varepsilon_S(x) - \varepsilon_{CS}(x)]\, dx \tag{8}$$

Neglecting the concrete contribution and referring to a linear variation in the steel stress along L_τ (Figure 6), it is possible to find:

$$w^t = \frac{\sigma_S^2 A_S}{\pi \phi \tau_m E_S} \tag{9}$$

In the present paper, Equation 9 is used to calculate the crack opening that generates steel yielding, w^t_y,

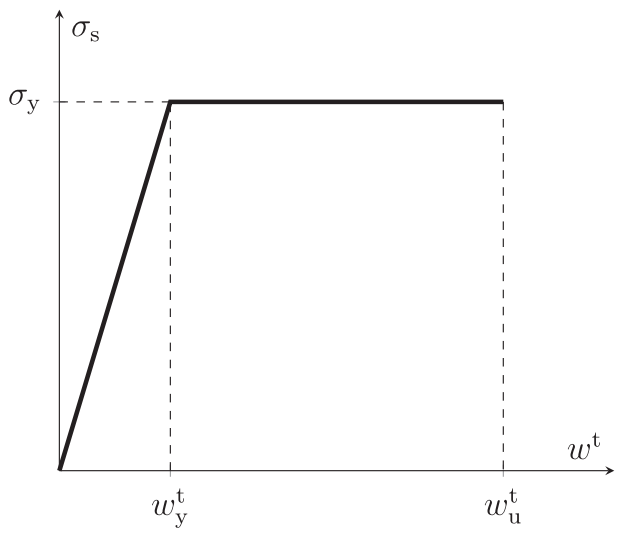

FIGURE 7 Steel constitutive law

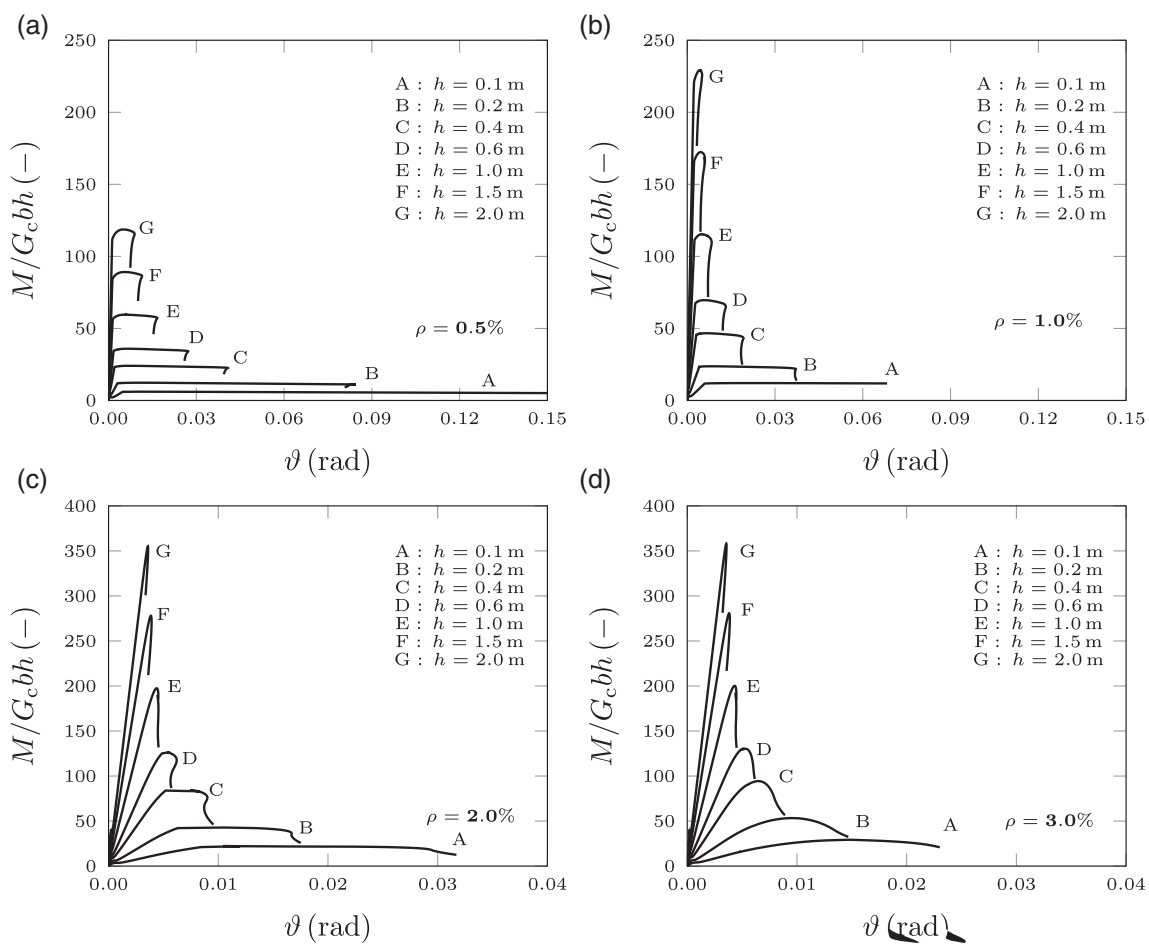

FIGURE 8 Dimensionless load versus rotation curves for RC beams: (a) $\rho = 0.5\%$, (b) $\rho = 1.0\%$, (c) $\rho = 2.0\%$, (d) $\rho = 3.0\%$

considering the following simplified elastic-perfectly plastic constitutive law for the steel reinforcement:

$$\sigma_s = \sigma_y \frac{w^t}{w_y^t} \tag{10}$$

σ_y being the yield strength of steel.

Furthermore, it is possible to evaluate the crack opening that generates steel fracture as:

$$w_u^t = \frac{\varepsilon_u \sigma_y A_s}{\pi \phi \tau_m} \tag{11}$$

Equation 10 and Equation 11 describe the steel constitutive law as depicted in Figure 7. It is important to note that Equation 5f coincides with Equation 10 only if the node r lies within the real crack length and if $w_r < w_y^t$

Within the Cohesive/Overlapping Crack Model numerical procedure, at each calculation step, the value of M is set as the minimum value of the bending moment that is able to generate the ultimate tensile force, F_t, in the fictitious tensile crack tip, m, or the ultimate compressive force, F_c, in the fictitious overlapping crack tip, p. Only the tip that firstly reaches the ultimate condition is moved to the following nodal point and calculation step, allowing the propagation of the cracking or crushing zone.

Then, the RC beam rotation is computed as:

$$\vartheta = \{K_M\}^T \{F\} + D_M M \tag{12}$$

$\{K_M\}$ being the vector containing the nodal displacements generated by a unit bending moment (Betti's Theorem) and D_M the coefficient of influence for $M = 1$.

3 | NUMERICAL VERSUS EXPERIMENTAL COMPARISON

In Figure 8, numerical curves obtained through the application of the Cohesive/Overlapping Crack Model to RC

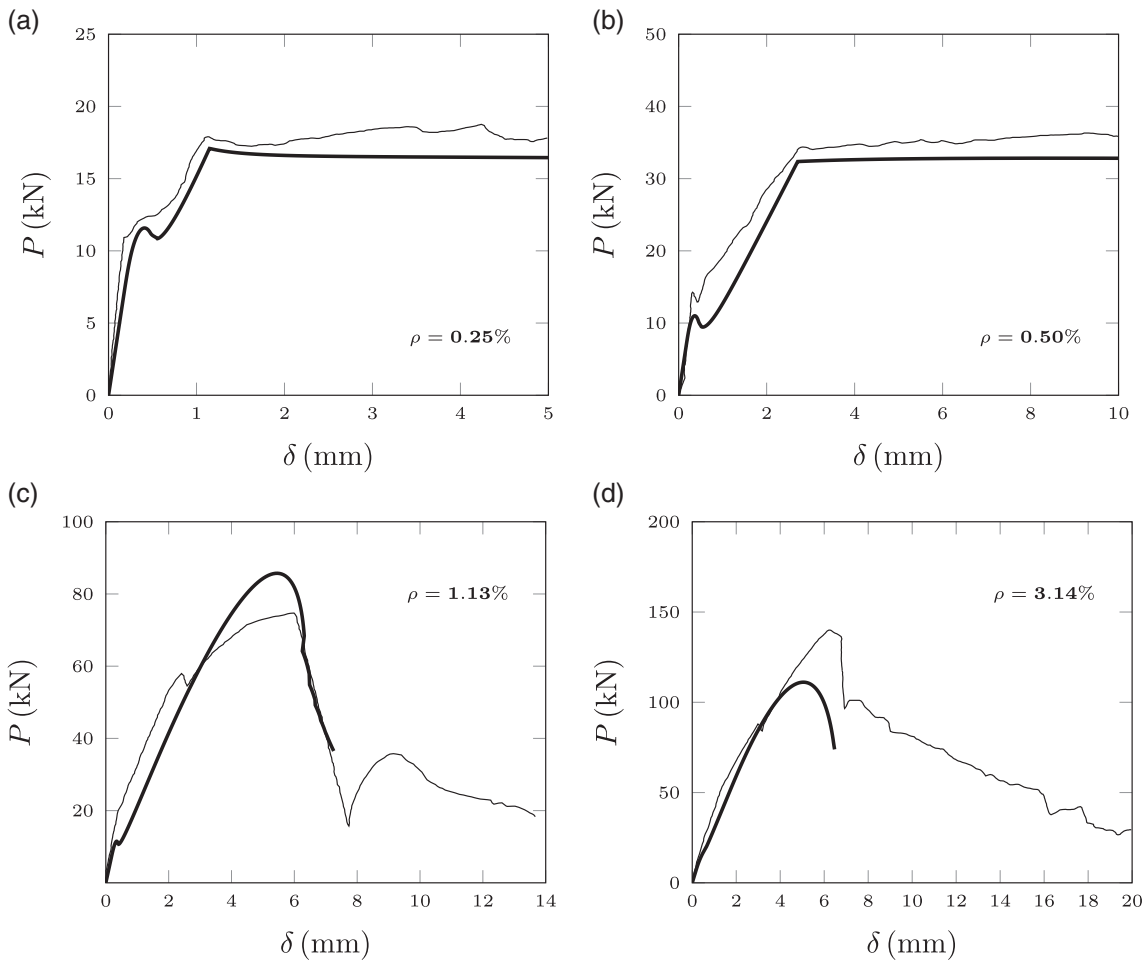

FIGURE 9 Numerical versus experimental comparison: (a) $\rho = 0.25\%$, (b) $\rho = 0.50\%$, (c) $\rho = 1.13\%$, (d) $\rho = 3.14\%$

beams in bending are presented. The curves describe the structural behavior of beams with thickness, b, equal to 0.2 m, and depth, h, varying between 0.1 and 2.0 m. The concrete matrix is assumed to have a compressive strength $\sigma_c = 40$ MPa, and a tensile strength $\sigma_t = 4$ MPa, whereas the fracture energy, G_F, and the crushing energy, G_c, are assumed equal to 0.08 and 30 N/mm, respectively. The steel yield strength $\sigma_y = 400$ MPa and the crack opening that generates steel yielding $w^t_y = 0.4$ mm have been assumed. On the other hand, the critical value generating steel fracture $w^t_u = 18.5$ mm has been calculated for a class B reinforcement (Eurocode 2).[42] In the numerical study of Figure 8, the reinforcement ratio, ρ, varies between 0.5% and 3.0%, and, for each reinforcement percentage, the ratio of the effective beam depth to the beam depth, d/h, is set equal to 0.9.

Figure 8(a) shows the curves obtained for $\rho = 0.5\%$. It is possible to observe that the rotational capacity, represented by the extension of the plastic plateau, decreases as the beam depth increases. For large beam depths, at the end of the plastic plateau it is possible to observe a catastrophic drop in the bearing capacity, generated by unstable propagation of the concrete crushing zone (snap-back), as it is also described in Figure 1. In Figure 8(b), the curves obtained for $\rho = 1.0\%$ are reported. This figure reveals a severe reduction in the extension of the plastic plateau for all the considered geometries, as well as a transition towards a more brittle behavior. The beams having $h = 1.5$ m and 2.0 m present a completely unstable behavior, since, once the maximum load is reached, a catastrophic loss in the bearing capacity occurs without steel yielding.

The reduction in the rotational capacity is also evident in Figure 8(c), where beams with $\rho = 2.0\%$ are analyzed: only the curves A-D present a plastic plateau. In Figure 8(d), all the curves present an unstable crushing behavior, a short plastic plateau being present only for $h = 0.1$ m.

In order to validate the abovementioned results, a numerical versus experimental comparison is performed by means of the Cohesive/Overlapping Crack Model. The experimental tests carried out by Carpinteri et al.[12] in order to investigate the ductile-to-brittle transition in RC beams are considered. These tests were performed on specimens having a cross-section of 100×200 mm^2 and a span of 1400 mm. The beams were casted using a concrete matrix characterized by $\sigma_c = 36.75$ MPa, $E = 33{,}058$ MPa, and $G_F = 0.112$ N/mm. Four different reinforcement percentages were investigated in the range $\rho = 0.25$–3.14%.

The numerical versus experimental comparison is presented in Figure 9. In Figure 9(a) and (b), the case-studies with $\rho = 0.25\%$ and $\rho = 0.50\%$ are analyzed, suggesting that the Cohesive/Overlapping Crack Model has a high capability in predicting concrete cracking, local snap-back instabilities, as well as steel yielding. Moreover, for large reinforcement percentages (Figure 9 (c) and (d)), a clear ductile-to-brittle transition is predicted by this Fracture Mechanics model.[43]

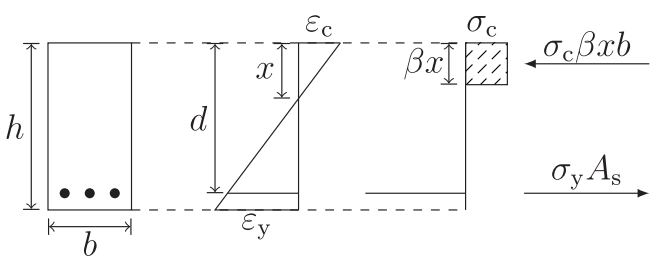

FIGURE 10 RC beam cross-section with balanced reinforcement percentage (Euler-Bernoulli theory)

4 | SCALE-DEPENDENCY OF THE MAXIMUM REINFORCEMENT PERCENTAGE

The numerical and experimental studies described in the previous section make evident the existence of an upper bound to the steel percentage, which is intended to avoid crushing and over-reinforcement. Such a steel percentage results to be scale-dependent (Carpinteri and Corrado[21]; Carpinteri et al.[35]). Currently, within the international standard requirements, a lack of knowledge exists about scale effects on RC maximum reinforcement conditions, since the maximum reinforcement percentage (also called "balanced reinforcement percentage") is trivially identified through the simplified Stress-block Model (Figure 10).

Hence, defining ε_c as the maximum deformation in concrete, and ε_y the deformation in steel at yielding, it is possible to find the neutral axis position in the section (Figure 10) as:

$$x = \frac{\varepsilon_c d}{\varepsilon_c + \varepsilon_y} \tag{13}$$

Indicating the depth of the stress block with βx, and imposing the equilibrium, it is possible to identify the maximum, or balanced, reinforcement percentage (Stress-block Model):

$$\rho_{max} = \frac{\sigma_c \beta}{\sigma_y h} \frac{\varepsilon_c d}{\varepsilon_c + \varepsilon_y} \tag{14}$$

On the other hand, for a more thorough vision of the problem, it is possible to perform a dimensional analysis

TABLE 1 Mechanical and geometrical parameters of the beams considered in the parametric study

σ_c (MPa)	σ_t (MPa)	G_F (N/mm)	G_c (N/mm)	E (GPa)	h (mm)	ρ (%)	s_c (–)	$N^u{}_P$ (–)
20	2.2	0.133	30	30	100	1.953	4.743	0.093
					200	1.841	3.354	0.123
					400	1.634	2.372	0.155
					800	1.360	1.677	0.182
					1600	1.114	1.186	0.211
					3200	0.917	0.839	0.246
35	3.2	0.144	30	34	100	2.828	2.886	0.126
					200	2.501	2.040	0.158
					400	2.112	1.443	0.188
					800	1.742	1.020	0.220
					1600	1.475	0.721	0.263
					3200	1.293	0.510	0.326
50	4.1	0.152	40	37	100	3.791	2.433	0.140
					200	3.280	1.720	0.172
					400	2.738	1.217	0.203
					800	2.259	0.860	0.236
					1600	1.961	0.608	0.290
					3200	1.754	0.430	0.367
65	4.5	0.158	49	40	100	4.672	2.154	0.150
					200	3.992	1.523	0.181
					400	3.315	1.077	0.213
					800	2.787	0.761	0.253
					1600	2.436	0.538	0.313
					3200	2.203	0.381	0.401
80	4.8	0.163	55	42	100	5.393	1.900	0.160
					200	4.568	1.343	0.191
					400	3.665	0.950	0.217
					800	3.242	0.672	0.271
					1600	2.873	0.475	0.340
					3200	2.626	0.336	0.440

through Buckingham's Theorem (Carpinteri and Accornero).[44] The resistance moment M developed by RC beams may be written as a function of several variables:

$$M = \Phi\left(\sigma_t, G_F, \sigma_c, G_c, E, \sigma_y, \rho, h; b/h, \ell/h, \vartheta\right) \tag{15}$$

E being the concrete elastic modulus and ℓ the beam span.

If we intend to avoid over-reinforced concrete beams, it is possible to neglect the variables G_F and σ_t, since the mechanical behavior of the abovementioned elements is mainly governed by the compressive strength and by the crushing energy of concrete. Thus, Equation 15 may be simplified as follows:

$$M = \Phi\left(\sigma_c, G_c, E, \sigma_y, \rho, h; b/h, \ell/h, \vartheta\right) \tag{16}$$

Assuming $(G_cE)^{0.5}$ and h as the independent variables, it is possible to rewrite Equation 16 as:

$$\frac{M}{\sqrt{G_cE}h^{2.5}} = \Phi_1\left(\frac{\sqrt{G_cE}}{\sigma_c h^{0.5}}, \rho\frac{\sigma_y h^{0.5}}{\sqrt{G_cE}}, \vartheta\frac{\sqrt{G_cE}}{Eh^{0.5}}\right) \tag{17}$$

where it is possible to recognize the Matrix Brittleness Number, $s_c = (G_cE)^{0.5}/\sigma_c h^{0.5}$, and the Reinforcement Brittleness Number, $N^U{}_P = \rho\sigma_y h^{0.5}/(G_cE)^{0.5}$.

Hence, through the application of the Cohesive/Overlapping Crack Model, it is possible to set up a parametric analysis in order to find the maximum reinforcement

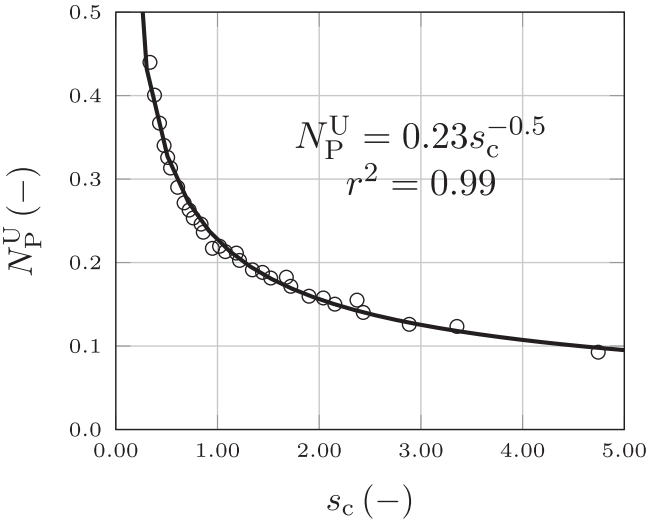

FIGURE 11 Upper bound ductile-to-brittle transition in RC beams

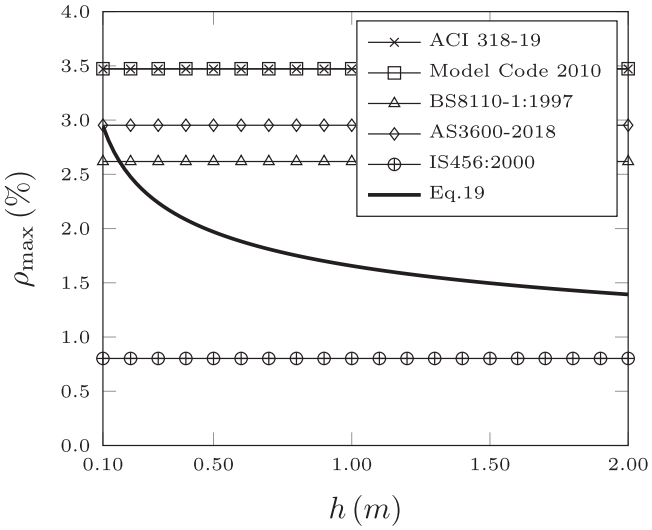

FIGURE 12 Comparison between different maximum reinforcement provisions

TABLE 2 Coefficients β and ε_c for the flexural resistance of RC beams

	β (−)	ε_c (−)
ACI 318–19[46]	0.85	0.003
Model Code 2010[39]	0.8	0.0035
Eurocode 2[42]	0.8	0.0035
BS8110-1:1997[47]	0.9 - applied stress in concrete 0.67 σ_c -	0.0035
AS3600-2018[48]	$0.65 < 0.85–0.007(\sigma_c\text{-}28) < 0.85$ - applied stress in concrete 0.85 σ_c -	0.003
IS456:2000[45]	0.36	0.0035

condition in the diagram s_c-N^U_P. The mechanical and geometrical parameters of the RC beams investigated in the present paper are reported in Table 1. Five different concrete grades were considered, and several beam depths were analyzed, spanning from $h = 0.1$ m to $h = 3.2$ m. For each RC beam, the ratio d/h is fixed at the value 0.9, whereas the steel yield strength is $\sigma_y = 450$ MPa. The fracture energy, G_F, was estimated through Model Code 2010[39], whereas the crushing energy, G_c, was calculated through Equation 2.

The calculated values of s_c and N^U_P are reported in Figure 11, where a best-fitting relationship provides:

$$N_P^U = 0.23 s_c^{-0.5} \tag{18}$$

Considering the definitions of s_c and N^U_P, it is possible to find:

$$\rho_{max} = 0.23 \frac{\sigma_c^{0.5} \left(\sqrt{G_c E}\right)^{0.5}}{\sigma_y h^{0.25}} \tag{19}$$

where an evident scale effect on the maximum reinforcement percentage is defined through the $h^{-0.25}$ power-law.

In Table 2, the β parameters and the ultimate strain of concrete, ε_c, provided by different international codes of practice are reported. It is possible to observe that all the considered provisions are rather similar, except for IS456:2000[45], which provides a smaller equivalent stress-block at Ultimate Limit State. Accordingly, in Figure 12 a comparison between the maximum reinforcement percentages provided by the above-mentioned standards and by Equation 19 are reported. This diagram clearly shows that all the current international codes do not take into account the scale effects on RC beams, providing a maximum reinforcement percentage far from that predicted by the Cohesive/Overlapping Crack Model and leading to a wrong assessment of the RC ductility.

5 | CONCLUSIONS

The application of the Cohesive/Overlapping Crack Model to the study of the maximum reinforcement percentage in RC beams provides a power law proportional to $h^{-0.25}$, being h the beam depth. The proposed formula for the assessment of an effective scale-dependent maximum reinforcement condition is compared to the current provisions given by several international standards,

outlining a clear shortcoming in the actual regulations concerning RC beams ductility. In such a framework, the Cohesive/Overlapping Crack Model may represent a powerful tool in the development of new design guidelines, which should reflect the real nature of concrete in a more rational and quantitative way, as also recently acknowledged by the American Association of State Highway and Transportation Officials.[49]

NOTATION

s_c	Matrix Brittleness Number
$N^U{}_P$	Reinforcement Brittleness Number
σ_t	tensile strength of concrete
ε_t	ultimate tensile strain of concrete
w^t	crack opening
$w^t{}_{cr}$	critical value of crack opening
G_F	fracture energy
σ_c	compressive strength of concrete
ε_c	ultimate compressive strain of concrete
w^c	fictitious interpenetration
$w^c{}_{cr}$	critical value of fictitious interpenetration
G_c	crushing energy
ε_{cs}	strain in concrete
ε_s	strain in steel
n	number of nodes
$\{w\}$	vector of nodal displacements
$[K_F]$	matrix of nodal displacements generated by unit forces
$\{F\}$	vector of nodal forces
$\{K_M\}$	vector of nodal displacements generated by unit bending moment
M	bending moment
ϑ	rotation
D_M	coefficient of influence for $M = 1$
h	beam depth
b	beam thickness
d	effective beam depth
ℓ	beam span
A_s	steel area
ρ	reinforcement percentage (A_s/bh)
ρ_{max}	maximum reinforcement percentage
σ_s	stress in steel
L_τ	transferring length
$\tau(x)$	shearing stress exchanged between steel and concrete
τ_m	mean value of the shearing stress exchanged between steel and concrete
Φ	bar diameter
E_s	steel elastic modulus
σ_y	steel yield strength
$w^t{}_y$	crack opening generating steel yielding
$w^t{}_u$	crack opening generating steel failure
x	depth of the neutral axis
β	ratio between stress block depth and neutral axis depth

DATA AVAILABILITY STATEMENT

Data sharing not applicable to this article as no datasets were generated or analysed during the current study

ORCID

Federico Accornero https://orcid.org/0000-0002-9638-8411

REFERENCES

1. Carpinteri A. Interpretation of the Griffith instability as a bifurcation of the global equilibrium. NATO ASI Series E: Appl Sci. 1985; 94:287–316. https://doi.org/10.1007/978-94-009-5121-1_10.
2. Carpinteri A. Cusp catastrophe interpretation of fracture instability. J Mech Phys Solids. 1989;37(5):567–582. https://doi.org/10.1016/0022-5096(89)90029-X.
3. Carpinteri A. Size effects on strength, toughness, and ductility. J Eng Mech (ASCE). 1989;115(7):1375–1392. https://doi.org/10.1061/(ASCE)0733-9399(1989)115:7(1375).
4. Carpinteri A, Accornero F. Multiple snap-back instabilities in progressive microcracking coalescence. Eng Fracture Mech. 2018; 187:272–281. https://doi.org/10.1016/j.engfracmech.2017.11.034.
5. Carpinteri A, Accornero F. The bridged crack model with multiple fibers: local instabilities, scale effects, plastic shake-down, and hysteresis. Theoretic Appl Fracture Mech. 2019;104. https://doi.org/10.1016/j.tafmec.2019.102351.
6. Carpinteri A, Accornero F. Residual crack opening in fibre-reinforced structural elements subjected to cyclic loading, Strength. Fracture Complex. 2020;12(2-4):63–74. https://doi.org/10.3233/sfc-190236.
7. Carpinteri A. Notch sensitivity in fracture testing of aggregative materials. Eng Fracture Mech. 1982;16(4):467–481. https://doi.org/10.1016/0013-7944(82)90127-8.
8. Carpinteri A. A fracture mechanics model for reinforced concrete collapse. Advanced Mechanics of Reinforced Concrete (Proceedings of a IABSE Colloqium). Delft, The Netherlands: Delft University Press; 1981. p. 17–30.
9. Carpinteri A. Sensitivity and stability of progressive cracking in plain and reinforced cement composites. Int J Cement Compos Lightweight Concr. 1982;4(1):47–56. https://doi.org/10.1016/0262-5075(82)90007-0.
10. Carpinteri A. Stability of fracturing process in RC beams. J Struct Eng (ASCE). 1984;110(3):544–558. https://doi.org/10.1061/(ASCE)0733-9445(1984)110:3(544).
11. Carpinteri A, Carmona JR, Ventura G. Failure mode transitions in reinforced concrete beams – part 1: theoretical model. Struct J (ACI). 2011;108:277–285.
12. Carpinteri A, Carmona JR, Ventura G. Failure mode transitions in reinforced concrete beams – part 2: experimental tests. Struct J (ACI). 2011;108:286–293.
13. CEB Bulletin 242. Ductility of Reinforced Concrete Structures, Comité euro-international du Béton (CEB). Switzerland: Lusanne; 1998.

14. Bigaj, A.J. (1999). Structural dependence of rotation capacity of plastic hinges in RC beams and slabs. PhD Thesis, Delft University of Technology, Delft, The Netherlands.
15. Bigaj AJ, Walraven JC. Size effect on the rotational capacity of plastic hinges in reinforced concrete beams. CEB Bulletin d'Information n. 218. Lusanne, Switzeland: Comité Euro-international du Béton (CEB); 1993. p. 7–24.
16. Debernardi PG, Taliano M. On evaluation of rotation capacity for reinforced concrete beams. Struct J (ACI). 2002;99(3):360–368.
17. Cohn MZ. Inelasticity of reinforced concrete and structural standards. J Struct Div (ASCE). 1979;105(11):122–146. https://doi.org/10.1061/JSDEAG.0005274.
18. Siviero E. Rotation capacity of monodimensional members in structural concrete. *CEB bulletin d'information n. 105*, Comité euro-internationale du Béton (*CEB*). Lusanne, Switzerland; CEB; 1976. p. 206–222.
19. Accornero F, Cafarelli R, Carpinteri A. Cracking and crushing in prestressed concrete beams. Struct J (ACI). 2021;118(2):101–109. https://doi.org/10.14359/51728184.
20. Accornero F, Cafarelli R, Carpinteri A. The cohesive/overlapping crack model for plain and RC beams: scale effects on cracking and crushing failures. Mag Concr Res. 2021. https://doi.org/10.1680/jmacr.20.00260.
21. Carpinteri A, Corrado M. Upper and lower bounds for structural design of RC members with ductile response. Eng Struct. 2011; 33(12):3432–3441. https://doi.org/10.1016/j.engstruct.2011.07.007.
22. Hawkins NM, Hjorteset K. Minimum reinforcement requirements for concrete flexural elements. In: Carpinteri A, editor. Application of Fracture Mechanics to Reinforced Concrete. London, UK: Elsevier; 1992. p. 379–412.
23. Ruiz G. Propagation of a cohesive crack crossing a reinforcement layer. Int J Fracture. 2001;111:265–282. https://doi.org/10.1023/A:1012260410704.
24. Ruiz G, Elices M, Planas J. Size effect and bond-slip dependence of lightly reinforced concrete beams. In: Carpinteri A, editor. Minimum Reinforcement in Concrete Members. Oxford, UK: Elsevier; 1999. p. 67–97. https://doi.org/10.1016/S1566-1369(99)80062-4.
25. Hillerborg A, Modéer P-EP. Analysis of crack formation and crack growth in concrete by means of fracture mechanics and finite elements. Cem Concr Res. 1976;6(6):773–781. https://doi.org/10.1016/0008-8846(76)90007-7.
26. Kotsovos MD. Effect of testing techniques on the post-ultimate behaviour of concrete in compression. Matériaux et Construct. 1983;6:3–12. https://doi.org/10.1007/BF02474861.
27. van Mier, J.G.M. (1984). Strain-Softening of Concrete under Multiaxial Loading Conditions. PhD thesis, Eindhoven University of Technology, Eindhoven, The Netherlands.
28. Vonk RA, Rutten HS, van Mier JGM, Fijneman HJ. Influence of boundary conditions on softening of concrete loaded in compression. In: Shah SP, Swartz SE, Barr B, editors. Fracture of Concrete and Rock - Recent Developments. New York, New York, USA: Taylor&Francis; 1989. p. 711–720.
29. van Mier JGM, Shah SP, Arnaud M, et al. Strain-softening of concrete in uniaxial compression. Materials and Structures. 1997;30(4):195–209. https://doi.org/10.1007/bf02486177.
30. Ferrara G, Gobbi ME. Strain softening of concrete under compression. Report to RILEM Committee 148. Enel-CRIS, Milan: Italy; 1995.
31. Jansen DC, Shah SP. Effect on length on compressive strain softening of concrete. J Eng Mech (ASCE). 1997;123(1):25–35. https://doi.org/10.1061/(ASCE)0733-9399(1997)123:1(25).
32. Akiyama M, Watanabe M, Abe S, Cui ST, Maeda N, Suzuki M. Compressive fracture behavior and mechanical properties of RC columns with normal and high-strength materials under concentric compression (in Japanese). Proc Japan Soc Civil Eng. 2006;62:477–496.
33. Suzuki M, Akiyama M, Matsuzaki H, Dang TH. Concentric loading test of RC columns with normal and high-strength materials and averaged stress-strain model for confined concrete considering compressive fracture energy. Proc 2nd Fib Congress. 2006.
34. Carpinteri A, Corrado M, Mancini G, Paggi M. The overlapping crack model for uniaxial and eccentric concrete compression tests. Mag Concr Res. 2009;61(9):745–757. https://doi.org/10.1680/macr.2008.61.9.745.
35. Carpinteri A, Accornero F, Cafarelli R. Ductile-to-brittle transition in RC and PC beams: scale effects on minimum and maximum reinforcements. In: Zhao B, Lu X, editors. Proceedings of the FIB symposium 2020. China: Shanghai; 2020. p. 1115–1162.
36. Carpinteri A, Corrado M, Paggi M. An integrated cohesive/overlapping crack model for the analysis of flexural cracking and crushing in RC beams. Int J Fracture. 2010;161: 161–173. https://doi.org/10.1007/s10704-010-9450-4.
37. Carpinteri A, Corrado M, Paggi M, Mancini G. New model for the analysis of size-scale effects on the ductility of reinforced concrete elements in bending. J Eng Mech (ASCE). 2009;135 (3):221–229. https://doi.org/10.1061/(ASCE)0733-9399(2009) 135:3(221).
38. Carpinteri A, Colombo G, Giuseppetti G. Accuracy of the numerical description of cohesive crack propagation. In: Wittmann FH, editor. Fracture Toughness and Fracture Energy of Concrete. Amsterdam, The Netherlands: Elsevier; 1986. p. 189–195.
39. fib (Fédération Internationale du Béton). Model Code for Concrete Structures 2010. New York, New York, USA: John Wiley & Sons; 2013.
40. Eligehausen R, Ozbolt J, Mayer U. Contribution of concrete between cracks at inelastic steel strains and conclusions for the optimization of bond. CEB Bulletin d'Information n. 242. Lusanne, Switzeland: Comité Euro-international du Béton (CEB); 1998. p. 275–295.
41. Langer P. The influence of HSC on the rotation capacity of plastic regions in RC structural members. CEB Bulletin d'Information n. 242. Lusanne, Switzeland: Comité Euro-international du Béton (CEB); 1998. p. 225–236.
42. CEN (European Committee for Standardization). Eurocode 2: Design of Concrete Structures – part 1–1: General Rules and Rules for Buildings. Brussels, Belgium: European Committee for Standardization; 2004.
43. Carpinteri A, Corrado M, Mancini G, Paggi M. Size-scale effects on plastic rotational capacity of reinforced concrete beams. Struct J (ACI). 2009;106:887–896.
44. Carpinteri A, Accornero F. Dimensional analysis of critical phenomena: self-weight failure, turbulence, resonance, fracture. Phys Mesomech. 2020;23(6):111–116. https://doi.org/10.24411/1683-805X-2020-16008.

45. BIS (Bureau of Indian Standards). Is 456:2000: Plain and Reinforced Concrete - Code of Practice. New Delhi, India: Bureau of Indian Standards; 2007.
46. ACI 318–19. Building Code Requirements for Structural Concrete (ACI 318–19). Farmington Hills, MI, USA: American Concrete Institute; 2019.
47. BS (British Standard) (1997). Structural use of concrete – Part 1: Code of practice for design and construction (BS 8110–1: 1997), British Standards.
48. AS3600:2018. Australian standard for concrete structures. Sydney, New South Wales, Australia: Standards Australia International Ltd; 2018.
49. AASHTO. LRFD Minimum Flexural Reinforcement Requirements. National Cooperative Highway Research Program (NCHRP) Research Report; 2019.

AUTHOR BIOGRAPHIES

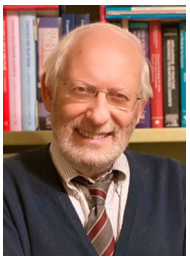

Alberto Carpinteri, Politecnico di Torino, Department of Structural, Geotechnical, and Building Engineering, Turin, Italy; Zhujiang (Pearl River)Professor of Guangdong Province, Department of Civil and Environmental Engineering, Shantou University, Shantou, P.R. China.

Federico Accornero, Politecnico di Torino, Department of Structural, Geotechnical, and Building Engineering, Turin, Italy.

Renato Cafarelli, Politecnico di Torino, Department of Structural, Geotechnical, and Building Engineering, Turin, Italy.

How to cite this article: Carpinteri A, Accornero F, Cafarelli R. Scale-dependent maximum reinforcement percentage in reinforced concrete beams. Structural Concrete. 2021;1–12. https://doi.org/10.1002/suco.202000573